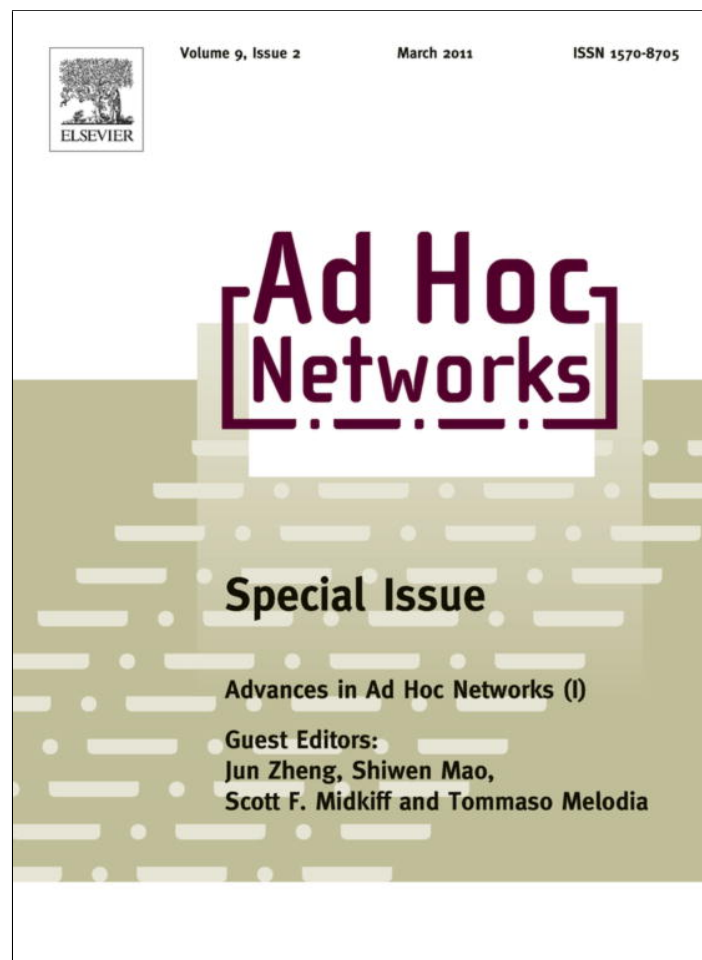


Provided for non-commercial research and education use.
Not for reproduction, distribution or commercial use.



This article appeared in a journal published by Elsevier. The attached copy is furnished to the author for internal non-commercial research and education use, including for instruction at the authors institution and sharing with colleagues.

Other uses, including reproduction and distribution, or selling or licensing copies, or posting to personal, institutional or third party websites are prohibited.

In most cases authors are permitted to post their version of the article (e.g. in Word or Tex form) to their personal website or institutional repository. Authors requiring further information regarding Elsevier's archiving and manuscript policies are encouraged to visit:

<http://www.elsevier.com/copyright>



Contents lists available at ScienceDirect

Ad Hoc Networks

journal homepage: www.elsevier.com/locate/adhoc

Contact time in random walk and random waypoint: Dichotomy in tail distribution

Chen Zhao*, Mihail L. Sichitiu

Department of Electrical and Computer Engineering, North Carolina State University, Raleigh, NC 27606, United States

ARTICLE INFO

Article history:

Available online 2 April 2010

Keywords:

Mobile Ad Hoc Network
 Random walk
 Random waypoint
 Contact time
 Dichotomy

ABSTRACT

Contact time (or link duration) is a fundamental factor that affects performance in Mobile Ad Hoc Networks. Previous research on theoretical analysis of contact time distribution for random walk models (RW) assume that the contact events can be modeled as either consecutive random walks or direct traversals, which are two extreme cases of random walk, thus with two different conclusions. In this paper we conduct a comprehensive research on this topic in the hope of bridging the gap between the two extremes. The conclusions from the two extreme cases will result in a power-law or exponential tail in the contact time distribution, respectively. However, we show that the actual distribution will vary between the two extremes: a power-law-sub-exponential dichotomy, whose transition point depends on the average flight duration. Through simulation results we show that such conclusion also applies to random waypoint.

© 2010 Elsevier B.V. All rights reserved.

1. Introduction

Due to the lack of real deployments of Mobile Ad Hoc Networks (MANETs), current research on this topic is still largely based on simulation. Therefore the behavior of mobility models greatly affects simulation performance [1]. Among numerous mobility models, Random Walk (RW) and Random Waypoint (RWP) are the most widely used ones [2,3] due to their simplicity, even though many researchers have pointed out that they have many drawbacks [4–6], and proposed several new ones [7–10,5]. However, even for the simple models like RW and RWP, the relationship between their input parameters (speed, pause, flight length, flight directions, etc.) and the corresponding impact on network performance is not yet quantitatively understood.

For dense MANETs with dynamic routing protocols, network performance depends on both the mobility and the protocols. In [1] the authors proposed several protocol

independent metrics including the link change rate and link duration, allowing the impact of mobility models to be evaluated through those metrics without reference to any specific protocol. For MANETs with sparser nodes, e.g., Pocket Switched Networks (PSN) [11], there are also such protocol independent metrics like the inter-contact time and the contact time [12].

In both scenarios the contact time (or alternatively, link duration, link lifetime, link expiration time, etc.¹) has been an important performance metric in evaluating the impact of mobility. In this paper we focus on the distribution of contact times of RW and RWP. Several papers studying this distribution have been published [13–21]. These works can be divided into three categories:

1. Study using simulation or empirical data [15,19].
2. Theoretical analysis that models contact events as single direct traverses [14,16–18].
3. Theoretical analysis that models contact events as sums of multiple i.i.d. random walks [13,20,21].

* Corresponding author. Tel./fax: +1 919 457 6589.

E-mail addresses: czhao4@ncsu.edu, chenzhao@ieee.org (C. Zhao), mlsichit@ncsu.edu (M.L. Sichitiu).¹ All these terms refer to the same metric. In this paper the term contact time is used.

Studies based on empirical analysis have the advantage of being accurate. In [15] the authors examined the PDFs of contact time through simulation and concluded that the PDFs are significantly different among different models. Among them the PDF of RW exhibits a single peak. The authors of [19] fit the PDF of contact time from RWP traces against several common distributions. The results showed that the lognormal distribution is the best fit for their traces.

Since it is very hard for the empirical analysis to go through all parameter spaces, theoretical derivation is necessary to better understand the underlying dynamics between the model parameters and the contact time, even though such derivation usually imposes simplifying assumptions. In RW and RWP, nodal movements are consecutive flights along straight lines. When the communication range is small in comparison to the flight length, it is reasonable to assume nodes do not stop or change directions during contact events. Thus the contact events are modeled as *direct traversals* [14,16–18]. In an early work [14] using this model, the duration distribution of two-hop paths with static sender and receiver was studied. In [16], the authors derived the contact time distribution of RW using the direct traversal model, assuming all nodes move at the same speed. In their later work [17] they extended the results with heterogeneous nodal speed. Both papers did not derive any closed form and all results were obtained numerically. In [18], the authors did a similar analysis as in [16] but derived a closed form for homogeneous speeds. They also obtained the contact time distribution numerically for two nodes with different fixed speeds.

On the other hand, when the communication range is large in comparison to the flight length, nodes often stop or change directions multiple times during contact events. Thus the contact events should then be modeled as the sum of *consecutive random walks* inside the nodes' communication range (usually modeled as circles) [13,20,21]. In an early work [13] using this model, the authors derived the probability of link availability with different initial conditions. In [20] the authors proposed a two-state Markovian framework that can be used to approximate the contact time distribution of any mobility model. They also stated that the “direct traversal” model is a special case in their framework. A comprehensive analysis of contact times using this model was done in [21], where the authors concluded that the contact time distribution can be approximated as exponential. In [21] the communication range is a random variable and the mobility model was a “smoothed” variation of RW [9]. As a special case, their conclusion also applies to ordinary RW with constant communication range.

However, both assumptions, direct traversal and consecutive random walk, are essentially two extremes in regarding the ratio of communication range and flight length. In general, the actual behavior of RW models lies in between the two extremes. In this paper we conduct a comprehensive analysis that bridge these two extreme assumptions in previous works. Especially, we investigate their difference in tail behavior. We first show that when flight lengths are infinite, which is equivalent to the direct

traversal assumption, the PDF of contact time has a power-law tail with both homogeneous and uniform speed distribution. Moreover, when flight lengths are no longer infinite, the contact time distribution shows a *power-law-sub-exponential dichotomy*, with the transition point being a function of the flight time distribution. As the average flight length becomes shorter, the transition takes place earlier. When, finally, the flight length is short enough in comparison to the communication range, which is equivalent to the consecutive random walk assumption, the dichotomy degenerates into a single exponential tail, which conforms to the conclusion in [21].

The rest of the paper is organized as follows: in Section 2 the main theoretical analysis is performed. The results are validated in Section 3. Section 4 concludes the paper.

2. Model analysis

In this section the mathematical analysis of the contact time distribution is presented. In Section 2.1 we present the basic settings and assumptions. In Section 2.2 we review the general derivation of contact time distribution in [16–18] for a simplified model assuming infinite flight lengths. In Section 2.3 the power-law tail behavior is investigated assuming both homogeneous and uniform speed distribution. In Section 2.4 we consider the impact of finite flight length and reach the conclusion of the power-law-sub-exponential dichotomy.

2.1. Model settings and assumptions

2.1.1. Random walk

In the RW model all nodes take consecutive random walks along straight line segments. These walks are called “flights”. For each flight a node travels in a direction ϕ at speed v for some distance u . Afterwards it pauses for some time t_p , and starts the next flight.

Flight parameters ϕ , v , u , and t_p are random variables selected independently for each flight. Also movements of different nodes are independent of each other. For most RW models, the direction ϕ is uniformly distributed over $[0, 2\pi]$, and the speed v is uniformly distributed over $[v_{\min}, v_{\max}]$ ($v_{\min} > 0$ as to obtain a stationary speed distribution [4]). The flight length u and pause time t_p can be fixed, or follow any common distributions like uniform, exponential or even power-law [5,22].

Throughout the analysis in this paper, all these assumptions for common RW models are used, except the pause time t_p is always ignored (fixed to zero). In addition, the nodal movements are confined to a taurus, which provides uniform node density and edge wrapping.

2.1.2. Random waypoint

RWP differs from RW in that for each flight every node selects a waypoint in a confined area instead of selecting the direction and the distance. Then the node travels to the waypoint through a straight line. Thus in RWP usually the node density is not uniform [23], the travel directions are not uniformly distributed, and the flight length distribution is determined by the shape of the confined area

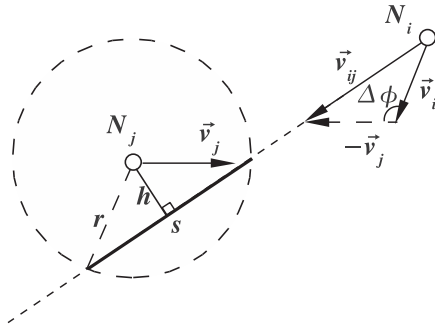


Fig. 1. A direct traverse contact event: N_i and N_j are moving at velocity \vec{v}_i and \vec{v}_j respectively. Both nodes have contact range r . From N_j 's perspective, N_i is traversing N_j 's communication range at the relative velocity \vec{v}_{ij} . The traversing trajectory is the thick solid chord s .

[24]. In addition, directions and distances of consecutive flights of the same node are not independent either. Therefore RWP is far more difficult to analyze than RW.

All analysis in this paper is based on the RW models, but the conclusions will also be validated against RWP through simulation in Section 3. The simulation results show that the conclusions obtained from RW hold sufficiently well for RWP.

2.1.3. Contact event

Every node is assumed to have the same symmetric communication range r , which is reasonable under most circumstances. Under such assumption when the distance between two arbitrary nodes N_i and N_j is smaller than r , the two nodes are considered to be able to communicate with each other, and vice versa. If during the time interval $[t_0, t_1]$ the nodes N_i and N_j are able to communicate with each other, while at the time instants t_0^- and t_1^+ they are not, then the time interval $[t_0, t_1]$ is referred to as a *contact event*, and its duration $t_1 - t_0$ is defined as the *contact time*.

2.2. Random walk with infinite flight length

We start with the assumption that all flights have infinite flight lengths so that the contact events are modeled as direct traversals as in [16–18]. More accurately, this is the limit case as the nodal flight lengths approach infinity.² Fig. 1 shows such a contact event. Nodes N_i and N_j are moving at velocity \vec{v}_i and \vec{v}_j , respectively. From N_j 's point of view, N_i is moving at the relative velocity:

$$\vec{v}_{ij} = \vec{v}_i - \vec{v}_j. \quad (1)$$

When N_i traverses N_j 's communication range (the dashed circle in Fig. 1), a contact event is generated. The duration is:

$$t_1 = \frac{s}{v_r} = \frac{s}{v_{ij}}, \quad (2)$$

² There is subtle difference between infinite and “approaching infinite” flight lengths. With strict infinite flight lengths, nodes never change their speeds so (11) does not hold. Since we are more interested in finding the limit when flight lengths approach infinity, we obtain the results here and in Section 2.3 assuming (11) holds.

where s is the traversing distance, which is the length of the chord, and v_r is the traversing speed *during a contact event*, which equals to the relative speed v_{ij} (but with different distributions, which will be explained in detail in Section 2.2.2), and t_1 is the contact time assuming infinite flight lengths.

The derivation of the distribution t_1 requires the distribution of both s and v_r . We also show that s and v_r are independent.

2.2.1. Distribution of s

Assume that node N_j is the reference frame. From N_j 's point of view, all other nodes N_i are moving at velocity $\vec{v}_{ij} = \vec{v}_i - \vec{v}_j$. All nodes with the same \vec{v}_{ij} are uniformly distributed on the plane and traversing N_j 's contact region with the same velocity $\vec{v}_r = \vec{v}_{ij}$. Thus, these traversing nodes we present here have their apothems h (Fig. 1) uniformly distributed over $[0, r]$. The chord s can be written as a function of apothem h :

$$s = 2\sqrt{r^2 - h^2} = g_s(h). \quad (3)$$

The pdf of h is (for pdf and cdf we use capitalized letters for subscripts):

$$f_H(h) = \begin{cases} \frac{1}{r} & 0 \leq h \leq r, \\ 0 & h > r. \end{cases} \quad (4)$$

Therefore the distribution of s given \vec{v}_r can be derived from (3) and (4) as follows:

$$f_{s|v_r}(s|v_r) = f_H(g_s^{-1}(s)) \left| \frac{d(g_s^{-1}(s))}{ds} \right|, \quad (5)$$

$$= \frac{s}{2r\sqrt{4r^2 - s^2}}. \quad (6)$$

The distribution of the chord s given v_r , $f_{s|v_r}(s|v_r)$, is independent of v_r , hence, s and v_r are *independent*. Thus the pdf of s is:

$$f_s(s) = \frac{s}{2r\sqrt{4r^2 - s^2}}. \quad (7)$$

2.2.2. Distribution of v_r

With two arbitrary nodes N_i and N_j , from (1) their relative speed v_{ij} is:

$$v_{ij} = |\vec{v}_{ij}| = |\vec{v}_j - \vec{v}_i| = \sqrt{v_i^2 + v_j^2 - 2v_i v_j \cos(\phi_j - \phi_i)}, \quad (8)$$

where v_i , v_j , ϕ_i , and ϕ_j are corresponding speeds and directions of \vec{v}_i and \vec{v}_j . For ease of computation we define the angle $\Delta\phi \in [0, \pi]$ so that $\cos(\Delta\phi) = \cos(\phi_i - \phi_j)$:

$$\Delta\phi = \cos^{-1}[\cos(\phi_i - \phi_j)]. \quad (9)$$

Thus

$$v_{ij} = \sqrt{v_i^2 + v_j^2 - 2v_i v_j \cos(\Delta\phi)}. \quad (10)$$

When v_i , v_j , and $\Delta\phi$ are mutually independent, the PDF of v_{ij} , denoted by $f_{v_{ij}}(v_{ij})$, can be derived from the distribution of v_i , v_j , and $\Delta\phi_i$ through multivariate transformation.

It is easy to prove that the angle $\Delta\phi$ is uniformly distributed on $[0, \pi]$. However, to derive the distribution of v_i and v_j is not trivial.

In RW or RWP the speed distribution can be defined in two different ways: the speed distribution that nodes use when choosing speeds at the beginning of each flight (uniform distribution for most RW models), or the speed distribution that would be obtained by randomly drawing node samples from the model. There are subtle differences between these two definitions. In [4,25] the authors pointed out that it takes some time for the model to reach a steady state (sometimes the model never reaches the steady state) so that the latter can be measured. We denote the former with $g_V(v)$ and the latter with $f_V(v)$. As long as speed is independent of flight length, the two distributions have the following relationship (see Appendix A.1 for derivation):

$$f_V(v) = \frac{\frac{1}{v}g_V(v)}{\int_{v_{\min}}^{v_{\max}} \frac{1}{v}g_V(v)dv}. \quad (11)$$

Since v_i and v_j in (10) are the speeds of arbitrarily drawn nodes, they have the distribution of $f_V(v)$ as shown in (11). Thus, the distribution of the relative speed v_{ij} is obtained through trivariate transformation:

$$f_{V_{ij}}(v_{ij}) = \int_{v_{\min}}^{v_{\max}} \int_{v_L}^{v_H} f_{V_i, V_j, V_{ij}}(v_i, v_j, v_{ij}) dv_i dv_j, \quad (12)$$

$$\text{where } f_{V_i, V_j, V_{ij}}(v_i, v_j, v_{ij}) = \frac{f_V(v_i)f_V(v_j)}{\pi} \left| \frac{\partial \Delta\phi}{\partial v_{ij}} \right|. \quad (13)$$

The integral intervals v_L and v_H of v_i are determined together by v_{\min} , v_{\max} , v_{ij} , and v_j .

Usually there is no closed form solution for (12). Even numerical results are not easy to obtain directly through (12). Alternatively, there is a more intuitive way to derive the PDF $f_{V_{ij}}(v_{ij})$ through polar coordinates (See Appendix A.2 for details).

Here v_{ij} is defined as the relative speed between two randomly chosen nodes and v_r is the relative speed between the two nodes during a *contact event*. The distribution of v_{ij} and v_r may not necessarily be the same because during a given period, there are more nodes with higher relative speeds traversing a node's contact area than nodes with lower speeds. From an arbitrary node N_j 's perspective, if the plane is filled with nodes with the same relative velocity \vec{v}_{ij} (Fig. 2), the number of nodes traversing N_j 's contact area during any given period is proportional to the relative speed v_{ij} . Therefore, the PDF of the relative speed v_r during *contact events* is:

$$f_{V_r}(v_r) = \frac{v_r f_{V_{ij}}(v_r)}{\int_0^{2v_{\max}} v_{ij} f_{V_{ij}}(v_{ij}) dv_{ij}}. \quad (14)$$

2.2.3. Distribution of t_i

Given (7) and (14) and the fact that they are independent, the PDF of the contact time assuming infinite flight length t_i can be derived through a random variable transformation:

$$f_{T_i}(t_i) = \int_0^{2v_{\max}} f_{V_r}(v_r) f_S(v_r t_i) v_r dv_r. \quad (15)$$

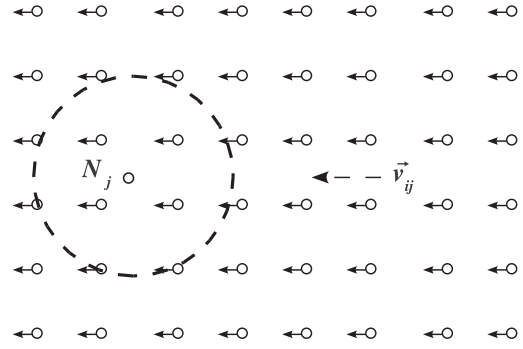


Fig. 2. From N_j 's perspective, when the plane is filled with nodes traversing at velocity \vec{v}_{ij} , the number of nodes traversed N_j 's contact area (the dashed circle) during a given period of time is proportional with the speed v_{ij} .

2.3. Tail behavior of contact time distribution

Generally the PDF of contact time in RW can only be obtained numerically through (15). However, most implementation of RW models assume homogeneous speeds or uniform speeds, thus when given infinite flight length the contact time distribution can be shown to have a power-law tail.

2.3.1. Random walk with homogeneous speeds

We start with a simplifying assumption that every node is moving at the same speed v_0 . With this assumption a closed form of the contact time distribution has been derived in [18]. Here we briefly obtain the same result using the formulas in Section 2.2.

With the homogeneous speed assumption the relative speed v_{ij} in (10) can be rewritten as:

$$v_{ij} = 2v_0 \sin \frac{\Delta\phi}{2} = g_V(\Delta\phi). \quad (16)$$

The angle $\Delta\phi$ is uniformly distributed over $[0, \pi]$. With a random variable transformation the PDF of the relative speed v_{ij} is:

$$f_{V_{ij}}(v) = f_\Phi(g_V^{-1}(v)) \left| \frac{d(g_V^{-1}(v))}{dv} \right|, \quad (17)$$

$$= \frac{2}{\pi \sqrt{4v_0^2 - v^2}}. \quad (18)$$

Substituting (18) into (14), the PDF of the relative speed during contact events is:

$$f_{V_r}(v) = \frac{v f_{V_{ij}}(v)}{\int_0^{2v_0} v f_{V_{ij}}(v) dv} = \frac{v}{2v_0 \sqrt{4v_0^2 - v^2}}. \quad (19)$$

Substituting (19), (7) into (15) the PDF of contact time can be derived:

$$f_{T_i}(t_i) = \int_0^{2v_0} f_{V_r}(v) f_S(v t_i) v dv = \frac{1}{4} \left(\frac{1}{t_0} + \frac{t_0}{t_i^2} \right) \log \frac{t_0 + t_i}{|t_0 - t_i|} - \frac{1}{2t_i}, \quad (20)$$

where $t_0 = \frac{r}{v_0}$.

The corresponding CDF of t_1 is:

$$F_{T_1}(t_1) = \int_0^{t_1} f_{T_1}(x) dx = \frac{1}{4} \left(\frac{t_1}{t_0} - \frac{t_0}{t_1} \right) \log \frac{t_0 + t_1}{|t_0 - t_1|} + \frac{1}{2}. \quad (21)$$

The PDF (20) has a maximum at t_0 . Then asymptotically (20) will follow a power-law distribution:

$$\begin{aligned} f_{T_1}(t_1) &= \frac{1}{4} \left(\frac{1}{t_0} + \frac{t_0}{t_1^2} \right) \log \frac{t_1 + t_0}{t_1 - t_0} - \frac{1}{2t_1} \\ &\cong \frac{1}{4} \left(\frac{1}{t_0} + \frac{t_0}{t_1^2} \right) \left(2 \frac{t_0}{t_1} + \frac{2}{3} \left(\frac{t_0}{t_1} \right)^3 \right) - \frac{1}{2t_1} \\ &\cong \frac{2t_0^2}{3t_1^3} \quad \text{when } t_1 \gg t_0. \end{aligned} \quad (22)$$

2.3.2. Random walk with uniform speed selection

For most common RW models nodes choose their speeds according to a uniform distribution on $[v_{\min}, v_{\max}]$ at the beginning of their flights. Under such a condition from (11) the nodal speed distribution is:

$$g_V(v) = \frac{1}{v_{\max} - v_{\min}}, \quad (23)$$

$$f_V(v) = \frac{1}{v \log H}, \quad \text{where } H = \frac{v_{\max}}{v_{\min}}. \quad (24)$$

From (10) the partial derivatives in (13) can be determined:

$$\Delta\phi = \cos^{-1} \frac{v_i^2 + v_j^2 - v_{ij}^2}{2v_i v_j}, \quad (25)$$

$$\frac{\partial \Delta\phi}{\partial v_{ij}} = \frac{2v_{ij}}{\sqrt{-v_i^4 - v_j^4 - v_{ij}^4 + 2v_i^2 v_j^2 + 2v_i^2 v_{ij}^2 + 2v_j^2 v_{ij}^2}}. \quad (26)$$

Substituting (24) and (26) into (13) and (12), the PDF of the relative speed v_{ij} can be written as:

$$\begin{aligned} f_{V_{ij}}(v_{ij}) &= \int_{v_{\min}}^{v_{\max}} \int_{v_L}^{v_H} \frac{2v_{ij} dv_i dv_j}{\pi v_i v_j \log^2 H} \\ &\quad \times \frac{1}{\sqrt{-v_i^4 - v_j^4 - v_{ij}^4 + 2v_i^2 v_j^2 + 2v_i^2 v_{ij}^2 + 2v_j^2 v_{ij}^2}}. \end{aligned} \quad (27)$$

The integral limits v_L and v_H in (27) are determined by not only v_{\min} and v_{\max} , but also the triangle law among v_i , v_j , and v_{ij} :

$$\begin{cases} v_i + v_j \geq v_{ij}, \\ v_i + v_{ij} \geq v_j, \\ v_j + v_{ij} \geq v_i. \end{cases} \quad (28)$$

The shape of the integral region varies as the value of v_{ij} varies. If only the asymptotic behavior of the contact time distribution is of interest, only the cases, where v_{ij} is small need to be considered, which simplifies the derivation. A typical such integral region is shown as the gray hexagon in Fig. 3 assuming $v_{ij} \leq \min(\frac{v_{\max} - v_{\min}}{2}, v_{\min})$. Since it is easier to do integral over a parallelogram than a hexagon, the upper and lower bound of $f_{V_{ij}}(v_{ij})$ are ob-

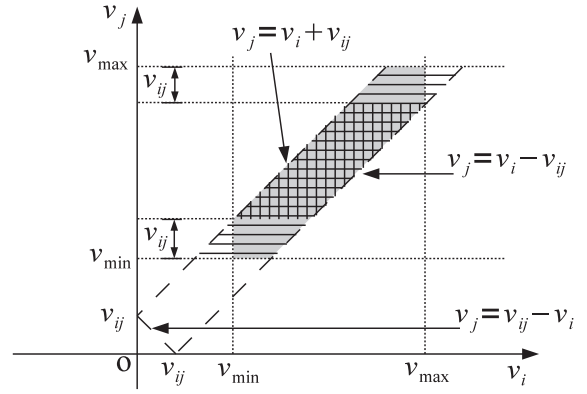


Fig. 3. An illustration of a typical integral interval for v_i and v_j in (27) assuming $v_{ij} \leq v_{\min}$. When v_{ij} is given, v_i and v_j have to satisfy (28) so the integral interval is the grey hexagon. Alternatively, the upper and lower bound of $f_{V_{ij}}(v_{ij})$ can be obtained by integration over the horizontally hatched area and vertically hatched area, respectively.

tained by taking integrals over the vertically hatched parallelogram and the horizontally hatched parallelogram in Fig. 3, respectively:

$$\begin{aligned} f_{V_{ij}}(v_{ij}) &< \int_{v_{\min}}^{v_{\max}} \int_{v_j - v_{ij}}^{v_j + v_{ij}} f_{V_i, V_j, V_{ij}}(v_i, v_j, v_{ij}) dv_i dv_j \\ &= \frac{\log \frac{v_{\max}^2 - v_{ij}^2}{v_{\min}^2 - v_{ij}^2} - 2 \log H}{2v_{ij} \log^2 H}, \end{aligned} \quad (29)$$

$$\begin{aligned} f_{V_{ij}}(v_{ij}) &> \int_{v_{\min} + v_{ij}}^{v_{\max} - v_{ij}} \int_{v_j - v_{ij}}^{v_j + v_{ij}} f_{V_i, V_j, V_{ij}}(v_i, v_j, v_{ij}) dv_i dv_j \\ &= \frac{\log \frac{v_{\max}^2 - 2v_{ij} v_{\max}}{v_{\min}^2 + 2v_{ij} v_{\min}} - 2 \log \frac{v_{\max} - v_{ij}}{v_{\min} + v_{ij}}}{2v_{ij} \log^2 H}. \end{aligned} \quad (30)$$

Applying the Taylor series:

$$f_{V_{ij}}(v_{ij}) < \frac{v_{ij} \left(\frac{1}{v_{\min}^2} - \frac{1}{v_{\max}^2} \right)}{2 \log^2 H} + O(v_{ij}^3), \quad (31)$$

$$f_{V_{ij}}(v_{ij}) > \frac{v_{ij} \left(\frac{1}{v_{\min}^2} - \frac{1}{v_{\max}^2} \right) - 2v_{ij}^2 \left(\frac{1}{v_{\min}^3} - \frac{1}{v_{\max}^3} \right)}{2 \log^2 H} + O(v_{ij}^3). \quad (32)$$

Substituting (31) and (32) into (14) the corresponding upper and lower bound for speed distribution during contact events $f_{V_r}(v_r)$ are:

$$f_{V_r}(v_r) < K_1 v_r^2 + O(v_r^4), \quad (33)$$

$$f_{V_r}(v_r) > K_1 v_r^2 - K_2 v_r^3 + O(v_r^4), \quad (34)$$

where K_1 and K_2 are constants. As $v_r \rightarrow 0$, the distribution of v_r approaches:

$$f_{V_r}(v_r) \cong K_1 v_r^2 + O(v_r^3). \quad (35)$$

Substituting (35) and (7) into (15) the asymptotic distribution of traverse time t_1 as $t_1 \rightarrow \infty$ is:

$$f_{T_1}(t_1) \cong \frac{K}{t_1^4}, \quad (36)$$

where K is a constant.

From (36) the contact time t_1 follows a power-law of t_1^{-4} with uniform speed selection, rather than the power-law of t_1^{-3} in (22) with homogeneous speed. Simulation results in Section 3.1 will show that the actual PDF tail of t_1 will first follow a power-law of t_1^{-3} as in (22), then switch to t_1^{-4} at some point. The larger the v_{\max}/v_{\min} ratio is, the sooner the transition takes place. The t_1^{-3} part will not be distinguishable when v_{\max}/v_{\min} is large.

2.4. Random walk with finite flight length

The analysis in previous sections is based on the assumption that nodal flight distances approach infinity such that contact events can be modeled as “direct traverses”. However, for most realistic scenarios and practical RW and RWP implementations, nodes will have finite flight lengths. For example, RWP in an $m \times m$ plane will have flight length distribution [24]:

$$f_U(u) = \begin{cases} \frac{2u^3}{m^4} - \frac{8u^3}{m^3} + \frac{2\pi u}{m^2} & u < m, \\ \frac{4u}{m^2} \left(\sin^{-1} \frac{m}{u} - \sin^{-1} \frac{\sqrt{u^2 - m^2}}{u} \right) & m \leq u \leq \sqrt{2}m, \\ -1 + \frac{2\sqrt{u^2 - m^2}}{m} - \frac{u^2}{2m^2} & m \leq u \leq \sqrt{2}m, \end{cases} \quad (37)$$

where u is the flight length. Typical RW models may have flight lengths following some standard distributions, like fixed length, uniform, exponential, power-law, etc. Recent studies [22,5] suggest that in the real world, human movements can be approximated by truncated levy walks.

Regardless of how flight lengths are distributed, the finite flight length will affect the contact time. Some of the traversing events will be interrupted because at least one of the two nodes finishes its flight and changes direction during the traversal. Intuitively, the longer a traversing event is, the more likely it would be interrupted. Once such interruption has reached a certain extent, the “direct traverse” assumption no longer holds and the contact time has to be modeled differently, e.g., as the sum of i.i.d random walks.

2.4.1. Traversal survival rate

To quantify the influence of finite flight length on the contact time, we first define the “survival rate” of direct traversing events. Given a direct traversing event, assume its duration is t_1 if nodes have infinite flight length (i.e., when the event is not interrupted), then when the flight length u is no longer infinite, the probability $\sigma(t_1)$ that the event *not* be interrupted is a function of t_1 . This probability is defined as the survival rate.

At the time of the start of a traversing event of duration t_1 , both nodes are at some place during their own flights. The traversing event will survive only if t_1 is no greater than any of the two residual flight times, where by residual flight time we refer to the remaining time in the current flight. As shown in Fig. 4, the traversal between N_1 and N_2 has a duration smaller than the residual flight time of N_1 , and thus it survives from N_1 's perspective (not necessarily from N_2 's perspective), while the one between N_1 and N_3 fails from N_1 's perspective. For convenience, we denote the survival rate from any single node's perspective with $\mu(t_1)$.

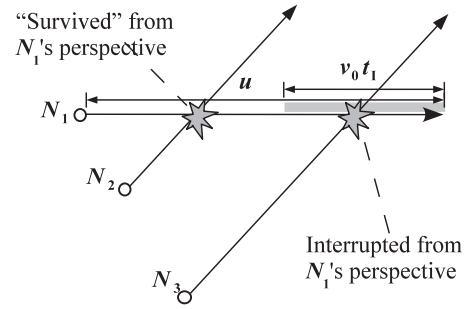


Fig. 4. Two traversing events: one between N_2 and N_1 and the other between N_3 and N_1 . When flight length is infinite, both events have duration t_1 . When the flight length u of N_1 becomes finite, the event between N_3 and N_1 is interrupted because N_1 stops before the traversal ends.

Since nodes are move independently of each other, survival from different nodes' perspectives are independent; we have:

$$\sigma(t_1) = \mu^2(t_1). \quad (38)$$

Given the PDF of flight length u , $f_U(u)$, the distribution used in selecting the flight speed v , $g_V(v)$ (which has the same meaning as the $g_V(v)$ in (11)), and the fact that u and v are independent, the PDF of the flight time t_U can be derived through a random variable transformation:

$$f_{T_U}(t_U) = \int_{v_{\min}}^{v_{\max}} g_V(v) f_U(v t_U) v dv. \quad (39)$$

Consider the flight of node N_1 in Fig. 4 with flight time t_U , a traversing event with uninterrupted duration t_1 occurs on this flight. Assume the occurrence probability of this event is uniformly distributed throughout the whole flight duration.³ Thus the probability that this traversing event “survives” from N_1 's perspective is:

$$\mu(t_1|t_U) = \begin{cases} \frac{t_U - t_1}{t_U} & t_1 < t_U, \\ 0 & t_1 \geq t_U. \end{cases} \quad (40)$$

Further, we assume that the occurrence density of traversing events (of the same t_1) along all flights is the same regardless of flight times or flight speeds.⁴ We denote this density with $\eta(t_1)$, and $\eta(t_1)$ is proportional to the PDF of t_1 in (15) ((15) is in fact the normalized form of $\eta(t_1)$). Therefore from (40) the expected numbers of “survived” events and total events of t_1 along that particular flight are:

$$M_{\text{total}} = \eta(t_1) t_U, \quad (41)$$

$$M_{\text{survive}} = \begin{cases} \eta(t_1) (t_U - t_1) & t_1 < t_U, \\ 0 & t_1 \geq t_U. \end{cases} \quad (42)$$

³ This assumption is true for most RW models, which have a uniform node density, but not strictly true for RWP, which has higher density in the center [23,25]. However simulation results show that this assumption holds sufficiently well for RWP.

⁴ This assumption is true for RW models with homogeneous speed. For those with heterogeneous speed, this assumption may not be accurate. However the results obtained here are shown to be good enough for heterogeneous speed case in simulation.

From (41) and (42) the survival rate (from a single node's perspective) $\mu(t_i)$ can be derived as the ratio between all the survived events with duration t_i and all events with the same duration t_i :

$$\begin{aligned} \mu(t_i) &= \frac{\int_{t_i}^{t_{Umax}} \eta(t_i)(t_U - t_i)f_{T_U}(t_U) dt_U}{\int_{t_{Umin}}^{t_{Umax}} \eta(t_i)t_U f_{T_U}(t_U) dt_U} \\ &= \frac{\int_{t_i}^{t_{Umax}} (t_U - t_i)f_{T_U}(t_U) dt_U}{E(t_U)}. \end{aligned} \quad (43)$$

From (38) and (43) the total survival rate for events with uninterrupted duration t_i is:

$$\sigma(t_i) = \mu^2(t_i) = \left(\frac{\int_{t_i}^{t_{Umax}} (t_U - t_i)f_{T_U}(t_U) dt_U}{E(t_U)} \right)^2. \quad (44)$$

It is hard to directly verify (44) through simulation. Practically (44) can be verified more accurately through the duration distribution of the "survived" traversing events, which is denoted with t_s :

$$f_{T_s}(t_s)C_{T_s} = f_{T_i}(t_s)\sigma(t_s), \quad (45)$$

$$C_{T_s} = \int_0^{t_{Umax}} f_{T_i}(t_s)\sigma(t_s) dt_s, \quad (46)$$

where C_{T_s} is a normalization factor.

2.4.2. Dichotomy in tail

Obviously (44) is a monotonically decreasing function: the longer a traversing event is, the more likely it is interrupted. When the survival rate $\sigma(t_i)$ falls below a certain threshold γ , the power-law tail of the contact time distribution no longer holds. The critical point that $\sigma(t_i)$ falls below γ is denoted with t_c :

$$\sigma(t_c) = \gamma. \quad (47)$$

Specifically, for RW with homogeneous speed v_0 , when flight lengths are fixed as u_0 ,

$$t_{Cfix} = \frac{u_0(1 - \sqrt{\gamma})}{v_0}. \quad (48)$$

When flight lengths are uniformly distributed over $[0, 2u_0]$,

$$t_{Cunif} = \frac{2u_0}{v_0}(1 - \sqrt[4]{\gamma}). \quad (49)$$

When flight lengths are exponentially distributed with mean u_0 ,

$$t_{Cexp} = -\frac{u_0}{2v_0} \log \gamma. \quad (50)$$

From simulations we found that the power-law-exponential transition takes place around $\gamma = 50\%$ for most RW and RWP models.

For contact events with duration longer than t_c , most of them will be interrupted and their actual duration may follow other distributions. Some of their actual duration may be less than t_c such that the power-law distribution for contact times smaller than t_c may also be distorted. However, since the tail is fast dropping (t^{-3} or t^{-4}), the total number of events with duration larger than t_c is small en-

ough compared to the number of shorter events so that this distortion can be neglected. Therefore, the tail behavior of contact time distribution for times smaller than t_c can still be considered as a power-law. Thus, the tail behavior of contact times will actually show a dichotomy: power-law before t_c , and something else thereafter.

In [26] the authors used a finite time renewing process to obtain the upper bound of inter-contact time distribution. The same technique can also be used here to obtain the upper bound of the contact time distribution. Assume nodes are moving on a finitely bounded surface with average flight length $E[t_U]$. Consider a node N_1 at the position $X_1(t_0)$ at time t_0 . After a period $t_R \gg E[t_U]$, it is reasonable to conclude that N_1 's position $X_1(t_0 + T)$ is independent of $X_1(t_0)$. From the stationary nodal distribution the probability that two nodes are within the contact range of one another is p_c . Thus the probability that two nodes N_1 and N_2 kept contact with each other for time T is:

$$P(t_i \geq T) \leq p_c^{T/t_R}, \quad (51)$$

which follows an exponential distribution. The parameter t_R is determined by both the boundary of the surface and the average flight time $E[t_U]$. The probability p_c is determined by both the average flight time $E[t_U]$ and the contact range r .

Thus, we conclude here that the contact time distribution for RW with finite flight lengths will exhibit a power-law-exponential dichotomy in their tail behavior, which is shown through simulations in Section 3.2.

Qualitatively, as average flight length $E[t_U]$ gets smaller, the power-law-exponential transition takes place earlier. When the average flight length become so small (usually smaller than the average contact range) that the power-law part is no longer distinguishable, the power-law-exponential dichotomy degenerates to a single exponential tail. In this case most contact events can be modeled as the sum of consecutive i.i.d. random walks, and a more accurate distribution is obtained in [21], where the PDF of contact times follow the exponential distribution:

$$f_{T_i}(t_i) \cong e^{-\lambda t_i}, \quad (52)$$

where

$$\lambda = \frac{E[v]}{r}. \quad (53)$$

$E[v]$ is the average nodal speed, and r is the contact range.

3. Validation

In this section the results in Section 2 are validated through simulation. In Section 3.1 we validate the conclusion of power-law tail assuming infinite flight lengths, and in Section 3.2 we validate the conclusion of dichotomy.

3.1. Infinite flight length without pause

The results derived in Sections 2.2 and 2.3 are in fact the limits as flight lengths approach infinity. Therefore, it is not appropriate to validate them against RW models with "true" infinite flight lengths, as in that case nodes never change their speeds or directions so (11) no longer holds. Since infinite flight length essentially equivalents to the

assumption that all traversing events are not interrupted, the results in Sections 2.2 and 2.3 should be better verified with the contact times collected by dividing the traversing lengths s by the speeds v_t during the same contact events from an RW or RWP model with finite flight lengths.

3.1.1. Closed forms for homogeneous speed

The closed forms (7), (19) and (21) for the homogeneous speed case are validated here ((7) applies to heterogeneous speed case, too.). Both an RW and an RWP model have been implemented with homogeneous speed and without pause. Both models used 100 nodes moving at $v = 1$ m/s with a contact range $r = 1$ m for 10 h. The RW model was on a taurus (implemented as a 10×10 m square with border wrapping) such that node density is uniform in all positions, and with the constant flight length of 50 m. The RWP model was on a 10×10 m square. Traversing lengths s and speeds v_t are collected for each traversing event, and the direct traversing time t_t is calculated from s and v_t . Their CDFs or CCDFs are plotted against the results from (7), (19) and (21) in Fig. 5.

In Fig. 5 the simulation results from both RW and RWP models (continuous and dashed lines) almost overlap with the theoretical values (dotted lines), as expected.

3.1.2. Tail behavior with heterogeneous speed

For heterogeneous speeds, theoretical results can only be obtained numerically. The tail behavior for RW models with uniform speed selection derived in (36) is verified here.

Simulations similar to those for homogeneous speed with infinite flight length were implemented but a uniform speed was selected at the beginning of each flight. Simulations were run with a constant average speed denoted by v_{avg} and different speed ranges H defined as follows:

$$g_V(v) = \frac{1}{v_{max} - v_{min}}, \quad (54)$$

$$H = \frac{v_{max}}{v_{min}}, \quad (55)$$

$$f_V(v) = \frac{\frac{1}{v} g_V(v)}{\int_{v_{min}}^{v_{max}} \frac{1}{v} g_V(v) dv} = \frac{1}{v \log H}, \quad (56)$$

$$v_{avg} = \int_{v_{min}}^{v_{max}} v f_V(v) dv = \frac{v_{max} - v_{min}}{\log H}. \quad (57)$$

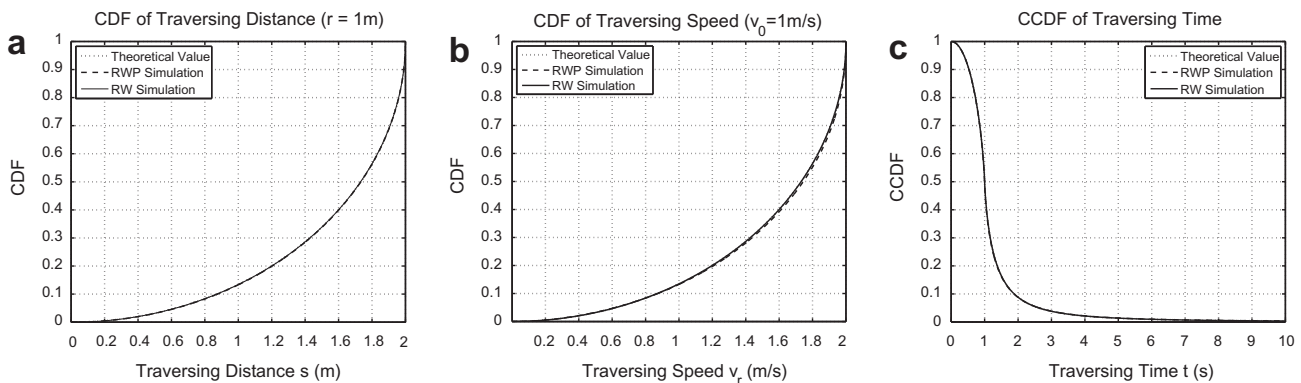


Fig. 5. Simulation results compared with theoretical results from (7), (19) and (21) (with homogeneous speed and no pause). (a) CDF of traversing length s , (b) CDF of traversing speed v_t , and (c) CCDF of traversing time t_t assuming no interruptions.

As with homogeneous speed, contact times were collected assuming infinite flight lengths by dividing traversing distances s by traversing speeds v_t from the same contact events. The CCDFs of contact times are shown in Fig. 6 on logarithmic scale.

The distribution of contact times in (36) can be validated in Fig. 6 as the distribution asymptotically approaches to t^{-4} rather than t^{-3} for the homogeneous speed case. As H becomes larger, the distribution approaches t^{-4} earlier.

3.2. Finite flight lengths without pause

The same models are used as in the previous section to validate the dichotomy conclusion in Section 2.4. Since the

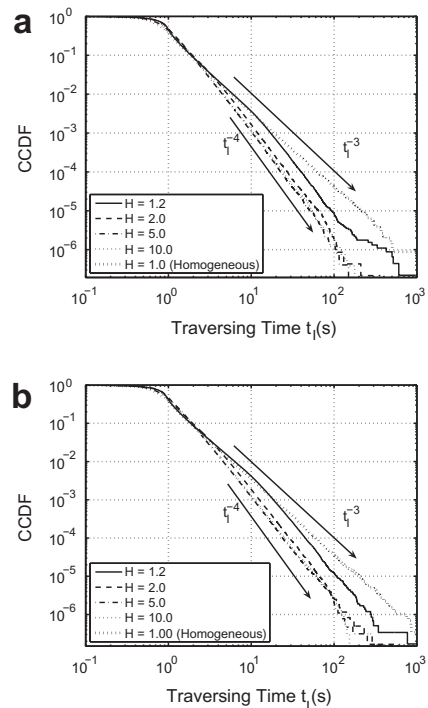


Fig. 6. Distribution of t_t with heterogeneous speed and without pause, with flight lengths approaching infinity (i.e., no interruptions in traversing events). Nodes select their speed at the beginning of each flight according to a uniform speed distribution. Different runs have the same average speed but different speed ranges. (a) Results based on the RW model and (b) results based on RWP.

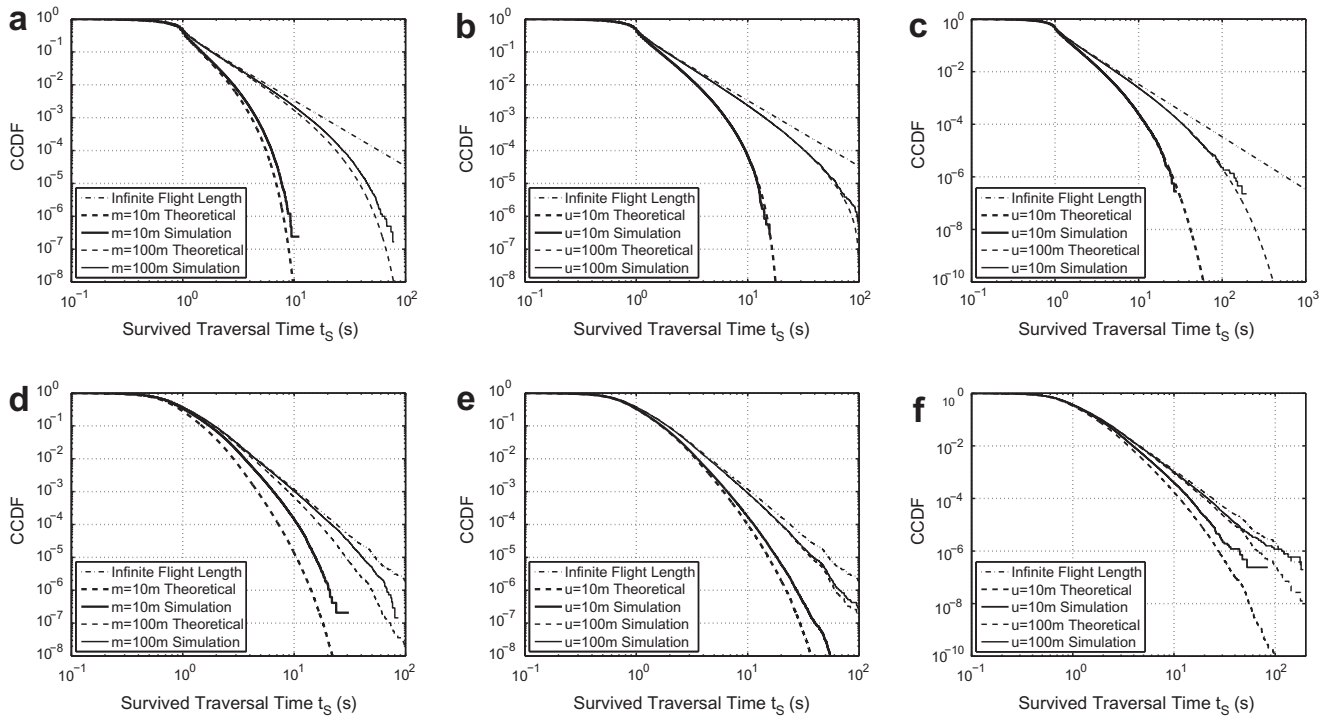


Fig. 7. CCDF of uninterrupted traversal duration t_s . Speed parameter $H = 1$ (homogeneous speeds) for (a)–(c) and $H = 10$ for (d)–(f). Mobility models: (a) and (d) RWP, (b) and (e) RWA, (c) and (f) RWB. All with contact range $r = 1$ m.

flight lengths are finite, we no longer calculate the traversal duration t_i , but instead directly measure the contact times t . We also diversify the random walk model by implementing different flight lengths: one RW model with uniform flight lengths on $[0, 2u]$, denoted with RWA; and one with exponential flight lengths with mean u , denoted with RWB. For the RWP model, we diversify its flight

lengths by varying its area $m \times m$. In addition, the contact range r is also set to different values to compare the results.

3.2.1. Traversal survival rate

We start by validating the traversal survival rate $\sigma(t_i)$ through the uninterrupted traversal duration t_s , whose PDF is derived in (45). The CCDFs of t_s are shown on

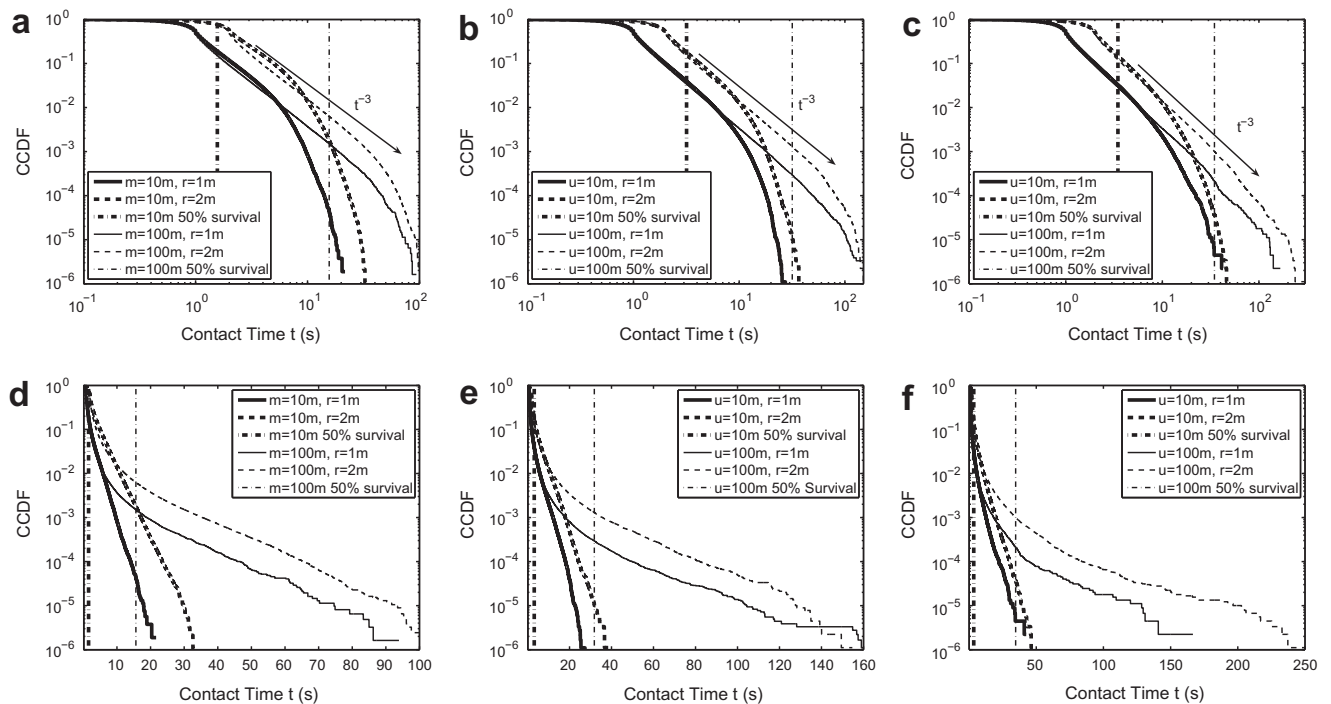


Fig. 8. CCDF of contact times for models with homogeneous speeds ($H = 1$) on logarithm plots (a)–(c) and semi logarithm plots (d)–(f). The vertical lines are the critical points t_c , where the survival rate $\sigma(t_c) = 50\%$. Mobility models: (a) and (d) RWP, (b) and (e) RWA, (c) and (f) RWB.

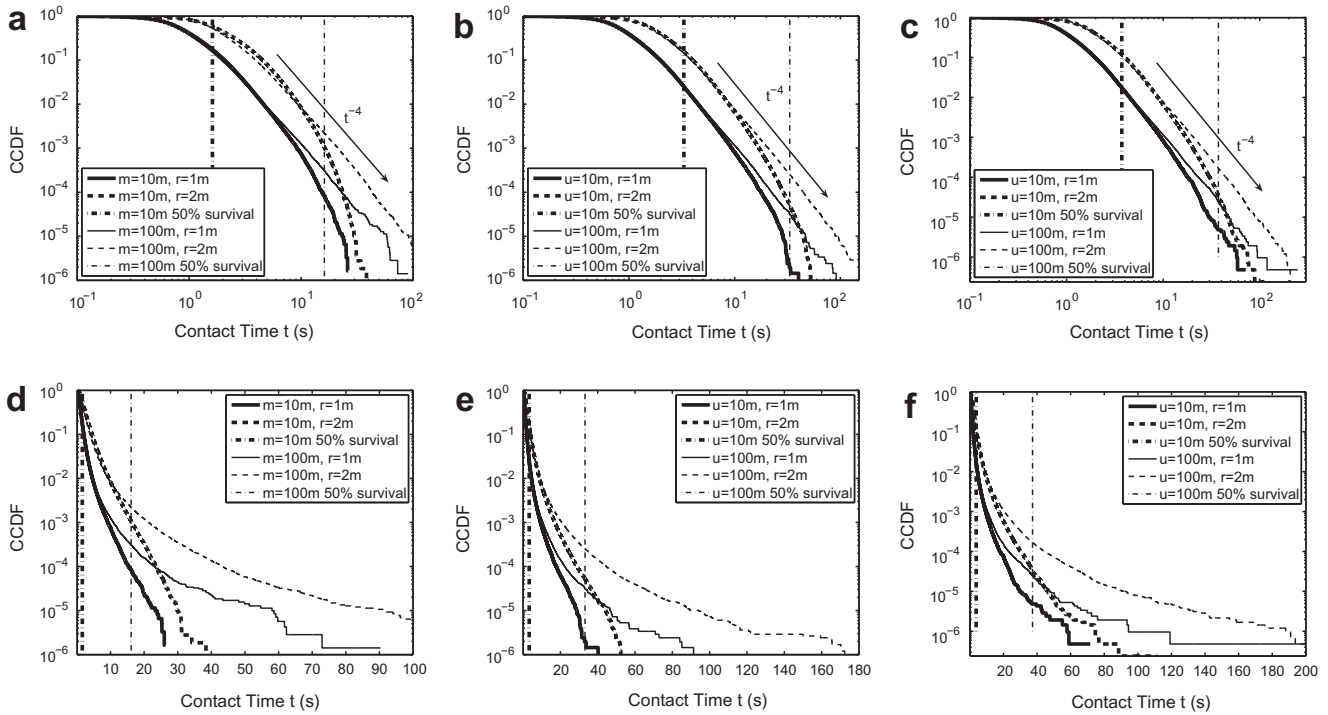


Fig. 9. CCDF of contact times for models with heterogeneous speeds ($H = 10$) on logarithm plots (a)–(c) and semi logarithm plots (d)–(f). The vertical lines are the critical points t_c , where the survival rate $\sigma(t_c) = 50\%$. Mobility models: (a) and (d) RWP, (b) and (e) RWA, (c) and (f) RWB.

logarithmic scale in Fig. 7 together with the theoretical results. It is shown that for all RW models with homogeneous speeds, the simulation results are very close to the theoretical predictions; but for RW with heterogeneous speeds or RWP models, there are slight differences between the theoretical and simulation results. That is due to the simplifying assumptions do not strictly hold true for RWP or heterogeneous speeds as discussed in Section 2.4. However, from the results shown, (44) still holds sufficiently well to reach the conclusion of dichotomy even with RWP or heterogeneous speed.

3.2.2. Dichotomy in the tail

The CCDFs of the contact time are plotted in Figs. 8 and 9 for models with different speed parameter H , contact range r and flight length u in both logarithmic scale and semi logarithmic scale. The critical points t_c where the survival rate $\sigma(t_c) = 50\%$ are also plotted as the vertical lines. From the logarithm plots the dichotomy is clearly shown in the tail of the CCDFs. When the same plots are shown on semi logarithm plots, the straight lines in the tail suggest the sub-exponential half of the dichotomy may be very close to exponential.

4. Conclusion and future work

In this paper we conducted a mathematical analysis of contact time distribution in random walk models, in the hope of bridging the gap between two existing approaches: the direct traversal model and the consecutive random walk model. We show that with uniform speed distribution under the direct traversal model the PDF of contact times has a power-law tail, while previous works show

an exponential tail under the consecutive random walk model. We conclude that for general random walks with uniform speed distribution, the PDF of contact times has a tail that is actually between the two extremes: a power-law-sub-exponential dichotomy, which degenerates into the extremes as the flight lengths vary. This conclusion is also validated against RWP models.

Since the parameters for the sub-exponential half of the dichotomy are still not quantitatively clear, a more comprehensive analysis for that part should be done in the future. Future work should also take the pause time into consideration, since it is one of the standard components of RW and RWP models. Also, the implication of such tail behavior of contact time distribution to MANET or DTN performance is also to be studied.

Acknowledgment

This research was supported by NSF Grant NSF-0626850.

Appendix A

A.1. Two definitions of speed distribution

Here we derive (11), the relationship between the two definitions of speed distribution. To facilitate the derivation, we start from a discrete speed distribution with M values, that is, $v \in (\xi_1, \xi_2, \dots, \xi_M)$. For simplicity assume there is only *one* node in the model, and the node has gone through N flights. We denote the length of the n th flight with s_n , and the speed driving that flight with v_n . We denote the probability that the node selects ξ_m as its speed

at the beginning of each flight with $P_g(\xi_m)$, and the probability that at any given time the node is traveling at the speed ξ_m with $P_f(\xi_m)$.

For each ξ_m , we define the set of flight indices that the flight is driven at the speed ξ_m :

$$\Xi_{m,N} = \{i | i \in \{1, \dots, N\} \text{ and } v_i = \xi_m\}, \quad (58)$$

such that the probability that the node is traveling at speed ξ_m is:

$$\begin{aligned} P_f(\xi_m) &= \lim_{N \rightarrow \infty} \frac{\sum_{i \in \Xi_{m,N}} S_i / v_i}{\sum_{n=1}^N S_n / v_n} = \lim_{N \rightarrow \infty} \frac{\frac{1}{\xi_m} \sum_{i \in \Xi_{m,N}} S_i}{\sum_{k=1}^M \frac{1}{\xi_k} \sum_{j \in \Xi_{k,N}} S_j} \\ &= \lim_{N \rightarrow \infty} \frac{\frac{1}{\xi_m} \frac{\sum_{i \in \Xi_{m,N}} S_i}{\sum_{n=1}^N S_n}}{\sum_{k=1}^M \frac{1}{\xi_k} \frac{\sum_{j \in \Xi_{k,N}} S_j}{\sum_{n=1}^N S_n}} = \frac{\frac{1}{\xi_m} P_g(\xi_m)}{\sum_{k=1}^M \frac{1}{\xi_k} P_g(\xi_k)}, \end{aligned} \quad (59)$$

where from the definition of $P_g(\xi_m)$:

$$P_g(\xi_m) = \lim_{N \rightarrow \infty} \frac{\sum_{i \in \Xi_{m,N}} S_i}{\sum_{n=1}^N S_n}. \quad (60)$$

Thus, at the limit the discrete (59) transforms to the continuous (11):

$$f_V(v) = \frac{\frac{1}{v} g_V(v)}{\int_{v_{\min}}^{v_{\max}} \frac{1}{v} g_V(v) dv}.$$

A.2. Alternative method to derive speed distribution

Here we present an alternative method to derive the relative speed distribution in (12) through polar coordinates, which is more intuitive and easier to calculate numerically.

It is intuitive to present the probability density of velocity $f_{\vec{v}}(\vec{v})$ on the polar coordinate as shown in Fig. 10, especially when directions are assumed to be independent of speed, and uniformly distributed over $[0, 2\pi]$ (as usually does in RW models). We denote the speed distribution with $f_V(v)$. The probability density of velocity \vec{v} of an arbitrary node N as shown in Fig. 10 is:

$$f_{\vec{v}}(\vec{v}) = \frac{1}{2\pi v} f_V(v) \quad \text{where } v = |\vec{v}|. \quad (61)$$

When two of such plots, corresponding to two arbitrary nodes N_i and N_j , are placed side by side as shown in Fig. 11, an arbitrary point A in the overlapping area will form a vector triangle with the two origins N_i and N_j , where $N_i A$ is \vec{v}_i , $N_j A$ is \vec{v}_j , and $N_i N_j$ is the relative velocity $\vec{v}_{ij} = \vec{v}_i - \vec{v}_j$. Thus, if the distance between the two origins N_i and N_j is set to their relative speed v_{ij} , the PDF of v_{ij} will be proportional to the integral of the joint probability density of \vec{v}_i and \vec{v}_j over the overlapping area (the double hashed area in Fig. 11):

$$f_{V_{ij}}(v_{ij}) = C_V \int_{\mathcal{A}(v_{ij})} f_{\vec{v}_i}(\vec{v}_i) f_{\vec{v}_j}(\vec{v}_j) dA, \quad (62)$$

where $\mathcal{A}(v_{ij})$ is the overlapping area, which is determined by v_{ij} . C_V is a normalization factor.

With (61) and (62) the PDF of the relative speed v_{ij} can be written in terms of the nodal speed distribution $f_V(v)$:

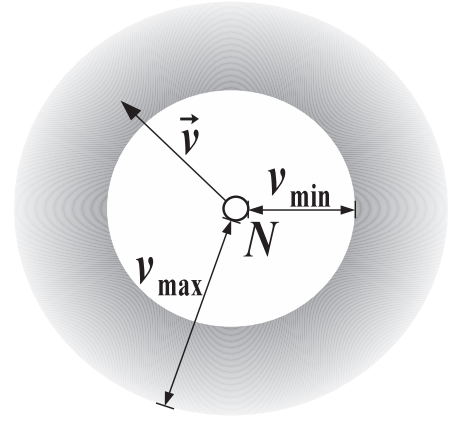


Fig. 10. Probability density of \vec{v} plotted on polar coordinate. The distance represents the speed, and the angle represents the direction. Darker shadow means higher probability density. Speed and direction are assumed to be independent of each other. Here speed is uniformly distributed over $[v_{\min}, v_{\max}]$, and direction is uniformly distributed over $[0, 2\pi]$.

$$f_{V_{ij}}(v_{ij}) = C_V \int_{\mathcal{A}(v_{ij})} \frac{f_V(v_i) f_V(v_j)}{4\pi^2 v_i v_j} dA, \quad (63)$$

where $v_i = |\vec{N}_i A|$ and $v_j = |\vec{N}_j A|$.

For most cases it is more intuitive and easier to obtain numerical results from (63) than directly through (12). For some special nodal speed distributions $f_V(v)$ even a closed form can be easily derived through (63). For example, one of those special speed distributions is the linear distribution:

$$f_V(v) = \frac{2v}{v_{\max}^2} \quad \text{where } 0 \leq v \leq v_{\max}. \quad (64)$$

Substituting (64) into (63), the closed form of $f_{V_{ij}}(v_{ij})$ is derived:

$$\begin{aligned} f_{V_{ij}}(v_{ij}) &= \frac{C_V}{\pi^2 v_{\max}^4} \int_{\mathcal{A}(v_{ij})} dA, \\ &= \frac{C_V}{\pi^2 v_{\max}^4} \left(2v_{\max}^2 \cos^{-1} \frac{v_{ij}}{2v_{\max}} \right. \\ &\quad \left. - v_{ij} \sqrt{v_{\max}^2 - \frac{v_{ij}^2}{4}} \right). \end{aligned} \quad (65)$$

Further, through (14) the PDF of v_r is:

$$f_{V_r}(v_r) = \frac{2v_r}{\pi v_{\max}^4} \left(2v_{\max}^2 \cos^{-1} \frac{v_r}{2v_{\max}} - v_r \sqrt{v_{\max}^2 - \frac{v_r^2}{4}} \right). \quad (67)$$

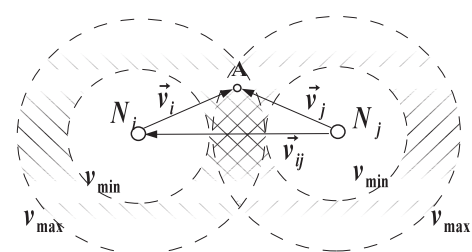


Fig. 11. Two plots from Fig. 10 with origin N_i and N_j are shown such that their shadows partially overlap (double hatched area). A is an arbitrary point in the overlapping area. Then $N_i A$, $N_j A$, and $N_i N_j$ will form a vector triangle, representing \vec{v}_i , \vec{v}_j , and \vec{v}_{ij} , respectively.

References

- [1] F. Bai, N. Sadagopan, A. Helmy, Important: a framework to systematically analyze the impact of mobility on performance of routing protocols for ad hoc networks, in: Proceedings of IEEE INFOCOM'03, San Francisco, CA, 2003.
- [2] T. Camp, J. Boleng, V. Davies, A survey of mobility models for ad hoc network research, *Wireless Communications and Mobile Computing* 2 (2002) 483–502.
- [3] F. Bai, A. Helmy, *Wireless Ad Hoc and Sensor Networks*, Kluwer Academic Publishers, Norwell, MA, 2004 (Chapter 1).
- [4] J. Yoon, M. Liu, B. Noble, Random waypoint considered harmful, in: Proceedings of IEEE INFOCOM'03, San Francisco, CA, 2003.
- [5] I. Rhee, M. Shin, S. Hong, K. Lee, S. Chong, On the levy-walk nature of human mobility, in: Proceedings of IEEE INFOCOM'08, Phoenix, AZ, 2008.
- [6] J. Yoon, M. Liu, B. Noble, Sound mobility models, in: Proceedings of ACM MOBICOM'03, San Diego, CA, 2003.
- [7] M. Kim, D. Kotz, S. Kim, Extract a mobility model from real user traces, in: Proceedings of IEEE INFOCOM'06, Barcelona, Spain, 2006.
- [8] M. Musolesi, C. Mascolo, Designing mobility models based on social network theory, *Mobile Computing and Communications Review* 11 (2007) 59–70.
- [9] M. Zhao, W. Wang, A novel semi-Markov smooth mobility model for mobile ad hoc networks, in: Proceedings of IEEE GLOBECOM'06, San Francisco, CA, 2006.
- [10] J. Yoon, B.D. Noble, M. Liu, M. Kim, Building realistic mobility models from coarse-grained traces, in: Proceedings of ACM MOBISYS'06, Uppsala, Sweden, 2006.
- [11] P. Hui, A. Chaintreau, J. Scott, R. Gass, J. Crowcroft, C. Diot, Pocket switched networks and human mobility in conference environments, in: WDTN '05: Proceedings of ACM SIGCOMM 2005 Workshop on Delay-Tolerant Networking, Philadelphia, PA, 2005.
- [12] A. Chaintreau, P. Hui, J. Crowcroft, C. Diot, R. Gass, J. Scott, Impact of human mobility on opportunistic forwarding algorithms, *IEEE Transactions on Mobile Computing* 6 (2007) 606–620.
- [13] A.B. McDonald, T. Znati, Link availability model for wireless ad-hoc networks. Technical report TR 99-07, University of Pittsburgh, Pittsburgh, PA, May 1999.
- [14] I. Gruber, H. Li, Link expiration times in mobile ad hoc networks, in: Proceedings of IEEE LCN'02, Los Alamitos, CA, 2002.
- [15] N. Sadagopan, F. Bai, B. Krishnamachari, A. Helmy, PATHS: analysis of path duration statistics and their impact on reactive MANET routing protocols, in: Proceedings of IEEE MOBIHOC'03, Annapolis, MD, 2003.
- [16] P. Samar, S.B. Wicker, On the behavior of communication links of a node in a multi-hop mobile environment, in: Proceedings of IEEE MOBIHOC'04, Roppongi, Japan, 2004.
- [17] P. Samar, S.B. Wicker, Link dynamics and protocol design in a multihop mobile environment, *IEEE Transactions on Mobile Computing* 5 (2006) 1156–1172.
- [18] C.-L. Tsao, Y.-T. Wu, W. Liao, J.-C. Kuo, Link duration of the random way point model in mobile ad hoc networks, in: Proceedings of IEEE WCNC'06, Las Vegas, NV, 2006.
- [19] A. Triviño-Cabrera, J. García-de-la-Nava, E. Casilari, F.J. González-Cañete, An analytical model to estimate path duration in MANETs, in: Proceedings of ACM MSWIM'06, Torremolinos, Málaga, Spain, 2006.
- [20] X. Wu, H.R. Sadjadpour, J. Garcia-Luna-Aceves, From link dynamics to path lifetime and packet-length optimization in MANETs, *Wireless Networks*.
- [21] W. Wang, M. Zhao, Joint effects of radio channels and node mobility on link dynamics in wireless networks, in: Proceedings of IEEE INFOCOM'08, Phoenix, AZ, 2008.
- [22] M.C. González, C.A. Hidalgo, A.-L. Barabási, Understanding individual human mobility patterns, *Nature* 453 (2008) 779–782.
- [23] C. Bettstetter, G. Resta, P. Santi, The node distribution of the random waypoint mobility model for wireless ad hoc networks, *Mobile Computing and Communications Review* 2 (2003) 257–269.
- [24] C. Bettstetter, H. Hartenstein, X. Pérez-Costa, Stochastic properties of the random waypoint mobility model, *Wireless Networks* 10 (2004) 555–567.
- [25] W. Navidi, T. Camp, Stationary distributions for the random waypoint mobility model, *IEEE Transactions on Mobile Computing* 3 (2004) 99–108.
- [26] H. Cai, D.Y. Eun, Crossing over the bounded domain: from exponential to power-law inter-meeting time in MANET, in: Proceedings of ACM MOBICOM'07, Montréal, Canada, 2007.



Chen Zhao was born in Suchow, China. He received a B.S. in Electrical Engineering with a minor in International Business from Shanghai Jiaotong University in 2006. He is currently a Ph.D. candidate in the Department of Electrical and Computer Engineering at North Carolina State University under the supervision of Dr Mihail Sichitiu. His research focuses on mobility models for wireless ad hoc networks.



Mihail L. Sichitiu was born in Bucharest, Romania. He received a B.E. and an M.S. in Electrical Engineering from the Polytechnic University of Bucharest in 1995 and 1996 respectively. In May 2001, he received a Ph.D. degree in Electrical Engineering from the University of Notre Dame. He is currently employed as an associate professor in the Department of Electrical and Computer Engineering at North Carolina State University. His primary research interest is in Wireless Networking with emphasis on ad hoc networking and wireless local area networks.